ON THE REACTION OF URANIUM(VI) AND THORIUM(IV) WITH PYROCATECHOL VIOLET

E. CHIACCHIERINI[a], R. GOCCHIERI[a] and L. SOMMER[b]

[a]*Department of Analytical Chemistry, University of Rome, Italy and*
[b]*Department of Analytical Chemistry, Purkyně-University, Brno*

Received January 27th, 1972

The equilibria of UO^{2+} and Th^{4+} with pyrocatechol violet were studied spectrophotometrically. Various mononuclear and dinuclear complexes of both metal ions are formed in solutions in dependence on the acidity and concentration of components. The spectrophotometric characteristics and equilibrium constants for various species were calculated.

Pyrocatechol violet (3,3′,4′-trihydroxyfuchson-2″-sulphonic acid, PCV) is an excellent non-selective metal indicator and chromogenic reagent widely used in the analytical practice[1-5]. In general, PCV resembles triphenylmethane dyes with *o*-hydroxyphenyl groupings in its behavior of analytical and complexing agent. For the reaction of pyrocatechol violet with uranyl[6] and with thorium[7] there exist only scarce data. There is a spectrophotometric method for the determination of thorium in slightly acidic solutions with which a number of cations and anions interfere[8]. PCV is also a promising metallochromic indicator for EDTA-titrations of thorium at pH 2·0—2·5 in the presence of 5-sulphosalicylic and ascorbic acids[9].

In this paper the reactions of uranium(VI) and thorium(IV) are studied spectrophotometrically in detail.

EXPERIMENTAL AND RESULTS

0·01M stock solution of uranyl sulphate (Merck, GFR) in 1M-$HClO_4$ was standardized gravimetrically *via* 8-hydroxyquinolinate. During further dilution the hydrolysis of UO_2^{2+} was avoided keeping the acidity of the diluted standard solutions not lower than 0·1M by perchloric acid. 0·01M stock solution of thorium nitrate (Merck, GFR) in 1M-$HClO_4$ was standardized *via* EDTA-titration. Because of easy hydrolysis of Th^{4+} the acidity of diluted standard solutions was kept not lower than 0·1M by perchloric acid.

Stock solutions of pyrocatechol violet (Merck, GFR) were prepared by dissolving the reagent in doubly distilled water. The reagent was doubly recrystallized from hot ethanol and contained 99% of active dye. Its purity was checked by elemental analysis, spectrophotometrically and by potentiometric titration with 0·1M-NaOH for two protons per reagent molecule. Fresh aqueous solutions were used only to which 1—2 drops of diluted ammonia were added to avoid formation of colloid particles in solution. The acidity of solutions was adjusted by dilute perchloric acid or ammonia (*i.e.* buffers were not used during complexation studies) and expressed in pH units or by the Hammett H_0-function related to perchloric acid[10,11]. The ionic strength $I = 0{\cdot}1$ was kept by sodium perchlorate with the exception of some measurements in stronger perchloric acid (Fig. 1).

Beckman DU or DK-2A spectrophotometers with standard silica cells and precision pH-meters PHM 22 Radiometer, Copenhagen or MEL 331A, Milan with standard glass and saturated calomel electrodes were used. All measurements were carried out at 25°C.

A similar graphical way of interpretation of absorbance data was used during these studies as in our previous work[12-15] especially using the slope-intercept and logarithmic transformations of the particular equilibrium constant derived and discussed earlier. Throughout the whole text the symbol pH denotes $-\log [H^+]$.

Acidobasic Equilibria of PCV

Various forms of the reagent are present in solutions, *i.e.* H_4L^-, H_3L^-, H_2L^{2-}, HL^{3-}, L^{4-} in dependence on acidity. The aqueous PCV solutions are red at pH 0·5, yellow at pH 1—5, violet at pH 6·5—8·5, red-violet at pH 9—11 and sky-blue at pH > 12. Distinct isosbestic points appear on the absorption curves for particular acidobasic equilibria (Fig. 1).

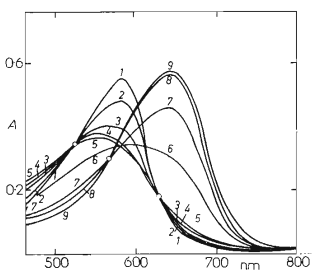

FIG. 1

Absorption Spectra of PCV in Dependence on Acidity

$c_L = 2{\cdot}00 \cdot 10^{-5}$M; 1% $NH_2OH.HCl$. pH: Curves *1* 9·6; *2* 9·9; *3* 10·4; *4* 10·8; *5* 11·0; *6* 12·0; *7* 12·8; *8* 13·6; *9* >14.

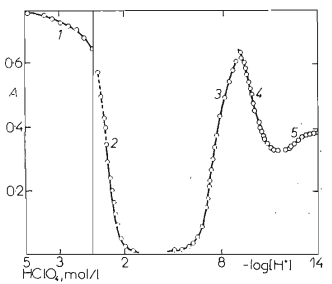

FIG. 2

Absorbance *vs* Acidity Plots of PCV Solutions

Curves *1*, *2* 550 nm, 4M-$NaClO_4$, c_L = $= 2{\cdot}00 \cdot 10^{-5}$M; *3* 590 nm, 0·1M-$NaClO_4$, $c_L = 2{\cdot}49 \cdot 10^{-5}$M *4*, *5* as *3*, with 1% NH_2OH. .HCl.

The absorbance *vs* acidity plots for various wave lengths were interpreted according to $\log \{(A - \varepsilon_{H_nL} c_L)/\varepsilon_{H_{n-1}L} c_L - A\}$ *vs* pH or H_0-transformations of the acid dissociation constant assuming that a particular equilibrium is solely constituted under selected conditions. Particular pH or H_0-intervals are to be seen from Figs 2, 3 and the optical characteristics and pK_a values are compared with those of previous authors[2,16-19] in Tables I—III. There is some doubt about the sequence of hydroxylic protons being liberated during the PCV dissociation but the following dissociation scheme is assumed:

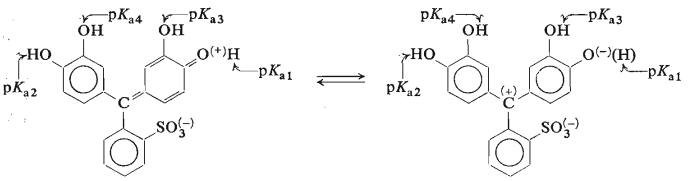

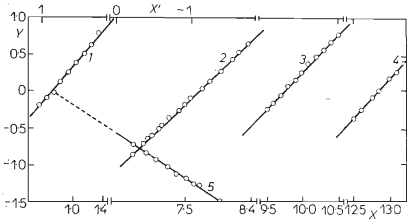

FIG. 3

Logarithmic Plots According to Eq. (5) *vs* pH

$Y = \log (A - \varepsilon_{H_nL} c_L)/(\varepsilon_{H_n} - \varepsilon_{1L} c_L - A)$. Curves *1* $c_L = 2{\cdot}00 \cdot 10^{-5}$M, 4M-$NaClO_4$, $X = -\log [H^+]$, *2* $c_L = 2{\cdot}49 \cdot 10^{-5}$M, 0·1M-$NaClO_4$, $X = pH$, *3*, *4* $c_L = 2{\cdot}00 \cdot 10^{-5}$M, 0·1M-$NaClO_4$, 1% $NH_2OH.HCl$, $X = pH$. *5* $c_L = 2{\cdot}00 \cdot 10^{-5}$M, 4M-$NaClO_4$, $X' = H_0$.

TABLE I

Optical Characteristics of Different Species of the Pyrocatechol Violet

Species	pH	Colour	λ_{max}, nm		
			this work	Ryba and coworkers[2]	Mustafin and coworkers[18]
H_5L^+ [a]	0	red	545	550	560
H_4L	0·5	red	550	550	—
H_3L^-	1—5	yellow	445	445	445
H_2L^{2-}	6·5—8·5	violet	590	590	600
HL^{3-}	9—11	red-violet	555—590	560	560—580
L^{4-} [b]	13	blue	645	560; 680[c]; 660[d]	[d]

[a] In 4M sodium perchlorate; [b] with 1% hydroxylamine hydrochloride, [c] according to ref.[17], [d] according to ref.[16].

TABLE II

Molar Absorptivities of Different Forms of PCV

Species	530 nm	550 nm	580 nm	590 nm	590[a]	600 nm
H_4L	$2{\cdot}95 \cdot 10^4$	$3{\cdot}70 \cdot 10^4$	—	—	—	—
H_3L^-	$1{\cdot}40 \cdot 10^3$	$1{\cdot}75 \cdot 10^3$	$4{\cdot}20 \cdot 10^2$	$4{\cdot}15 \cdot 10^2$	—	$4{\cdot}00 \cdot 10^2$
H_2L^{2-}	$1{\cdot}80 \cdot 10^4$	$2{\cdot}25 \cdot 10^4$	$3{\cdot}00 \cdot 10^4$	$3{\cdot}03 \cdot 10^4$	$3{\cdot}60 \cdot 10^4$	$2{\cdot}96 \cdot 10^4$
H_2L^{3-}	—	—	—	—	$1{\cdot}60 \cdot 10^4$	—
L^{4-}	—	—	—	—	$2{\cdot}00 \cdot 10^4$	—

[a] With 1% of $NH_2OH.HCl$.

TABLE III

Dissociation Constants (pK_{an}) for Acid-Base Couples of PCV

pK_a	Species	Isosbestic points (this work)	pK_{an} this work	Ryba and coworkers[2]	Wang and coworkers[2]	Mustafin and coworkers[18]
pK_{a1}	H_4L/H_3L^-	488	$0{\cdot}8 \pm 0{\cdot}1$[a]	—	—	—
pK_{a2}	H_3L^-/H_2L^{2-}	492	$7{\cdot}80 \pm 0{\cdot}02$[a]	7·81[a]; 7·82[b]	7·8[c]	6·91[a]
pK_{a3}	H_2L^{2-}/HL^{3-} [d]	525—630	$9{\cdot}76 \pm 0{\cdot}02$[a]	9·80[a]; 9·76[b]	10·1[c]	7·87[a]
pK_{a4}	HL^{3-}/L^{4-} [d]	568	$12{\cdot}8 \pm 0{\cdot}1$[a]	11·73[b]; 12·50[b,e]	—	10·84[a]

[a] Spectrophotometry; [b] potentiometry; [c] polarography; [d] solutions with 1% (w/v) hydroxylamine hydrochloride; [e] *cf.* ref.[16]. Recently following values were also published: pK_{a2} 7·90; pK_{a3} 9·94; pK_{a4} 11·82 (for $I = 0{\cdot}1$)[30].

There is some optical evidence for the protonated H_5L^+ form in strongly acidic medium such as 7—10M-$HClO_4$, where the $-SO_3^-$ group is protonated. In turn the protonation of H_3L^-, corresponding to the protonation of the quinoid oxygen, is controlled by a single proton equilibrium till 4M perchloric acid (Fig. 3, curve *5*). In strongly alkaline medium the reagent is easily oxidized which causes a hypsochromic shift of the absorption maximum and colour fading with time. The excess of hydroxylamine or hydrazine hydrate can serve as sufficient protective. The pH interval 1·5—6·0 is most promising for complexation studies because of large optical contrast between the yellow reagent form H_3L^- (λ_{max} 445 nm) and the metal complexes formed.

THE SYSTEM UO_2^{2+}–PYROCATECHOL VIOLET

The reaction between UO_2^{2+} and PCV occurs at pH > 2·5 at room temperature where soluble coloured complexes are formed. The solutions with excess of uranyl ions show λ_{max} 550 nm

at pH 3·0 but a λ_{max} 620 nm at pH > 4·0. There is only one λ_{max} 550 nm for solutions with excess of ligand at pH < 6·0. This is an evidence for the existence of more than one UO_2^{2+}-complex with PCV under various conditions.

Solutions with excess of UO_2^{2+} *ion*: The acidity *vs* absorbance curves of the PCV—UO_2^{2+} system show different shapes depending on wave length (Fig. 4) which is an evidence of the existence of at least two complexes in this case. Respecting the equilibrium (*A*) following transformations are valid (the charge of complexes is omitted):

$$m\,M + n\,H_xL \rightleftarrows M_mL_nH_z + q\,H^+ ; \quad {}^*\beta_{nm} \qquad (A)$$

$$c_L/(A - A_M) = n/\varepsilon_n + \{[Z(A - A_M) - \bar{\varepsilon}c_L]\,[n\bar{\varepsilon}_L - Z\varepsilon_n]^{n-1}\,[H]^q\}/(A - A_M)\,.$$
$$.\,[\bar{\varepsilon}_n c_L - n(A - A_M)]^{n-1}\,{}^*\beta_{nm}\varepsilon_n^q c_M^m \qquad (1)$$

or

$$A - A_M = \varepsilon_n c_L - \{[(A - A_M)\,Z - \bar{\varepsilon}_L c_L]\,[H]^q/c_M^m\,{}^*\beta_{nm}\} \qquad (2)$$

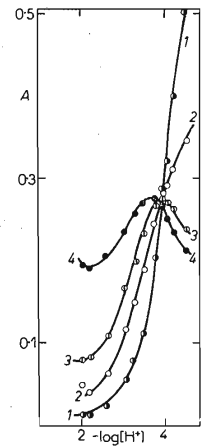

FIG. 4

Absorbance *vs* pH plots for PCV Solutions in the Presence of Uranyl Ion Excess

$c_L = 2{\cdot}00 \,.\, 10^{-5}$M, $c_M = 4{\cdot}00 \,.\, 10^{-3}$M. Curves *1* 600 nm, *2* 560 nm, *3* 530 nm, *4* 500 nm.

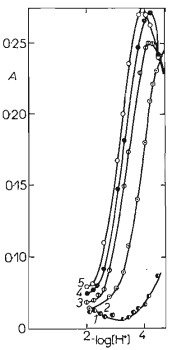

FIG. 5

Absorbance *vs* pH Plots for PCV Solutions with Various Uranyl Ions Excess

530 nm, $c_L = 2{\cdot}00 \,.\, 10^{-5}$M. Curves *1* $c_M/c_L = 1$, *2* $c_M/c_L = 20$, *3* $c_M/c_L = 80$, *4* $c_M/c_L = 150$, *5* $c_M/c_L = 200$.

considering the partial dissociation of the ligand:

$$H_xL \rightleftarrows H_{x-1}L + H^+ ; \quad K_{ax} . \qquad (A1)$$

If H_xL reacts:

$$\bar{\varepsilon}_L = \varepsilon_{H_xL} + \varepsilon_{H_{x-1}L}[H]/K_{ax} ; \quad Z = 1 + K_{ax}/[H] \qquad (3)$$

and in the case of reaction of $H_{x-1}L$:

$$\bar{\varepsilon}_L = \varepsilon_{H_{x-1}L} + \varepsilon_{H_xL}K_{ax}/[H] ; \quad Z = 1 + [H]/K_{ax} . \qquad (4)$$

The increasing part of the absorbance *vs* pH plot at 530 nm for solutions with $c_M/c_L \sim 20-200$ was analyzed according to (*1*) and (*2*) to test the occurrence of the usual equilibria (*B*) and (*C*) (Fig. 5):

$$M + H_3L \rightleftarrows MH_2L + H^+ , \qquad (B)$$

$$M + H_3L \rightleftarrows MHL + 2H^+ . \qquad (C)$$

The hydrolysis of the UO_2^{2+} ions alone could interfere with the equilibria at pH > 4 only as a result of the increasing concentration of UO_2^{2+} in solution[20,21]. The transformations (*1*) and (*2*) represent straight lines for $q = 1$ and $n = 1$ (Fig. 6). The

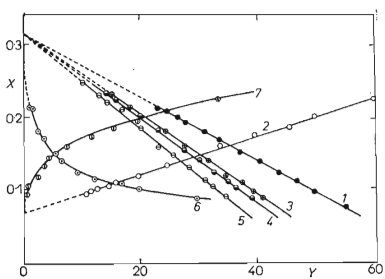

FIG. 6

Analysis of the Increasing Part of the Absorbance *vs* pH Plots According to Eq. (*1*), (*2*)
Experimental conditions the same as in Fig. 5. Curves: *1* $c_M/c_L = 20$; $X = A$; $Y = \{(A - A_L)[H]/c_M\} . 10^3$; *2* $c_M/c_L = 20$; $X = (c_L/A) . 10^7$; $Y = [(A - A_L)[H]/A . c_M]$; *3* $c_M/c_L = 80$; $X = A$; $Y = \{(A - A_L) . [H]/c_M\} . 10^3$; *4* $c_M/c_L = 150$; $X = A$; $Y = \{(A - A_L)[H]/c_M\} . 10^2$; *5* $c_M/c_L = 200$; $X = A$; $Y = \{(A - A_L)[H]/c_M\} . 10^3$; *6* $c_M/c_L = 20$; $X = A$; $Y = (A - A_L)[H]^2/c_M$; *7* $c_M/c_L = 20$; $X = c_L/A$; $Y = (A - A_L) . [H]^2/A . c_M$.

logarithmic analysis of the increasing part of the absorbance *vs* pH plots according to the derived equation (*5*):

$$\log \{[Z(A - A_M) - \bar{\varepsilon}_L c_L]/[\varepsilon_n c_L - n(A - A_M)]^n\} =$$

$$= m \log c_M - q \log [H] - (n - 1) \log (n\bar{\varepsilon}_L - Z\varepsilon_n) + \log {}^*\beta_{nm}, \qquad (5)$$

into which the values of ε_n from the intercepts of the Eq. (*1*) and (*2*) were inserted, leads to straight lines with monotonous slopes, $q = 1$, if $n = 1$ is assumed again (Fig. 7). The set of absorbance *vs* pH curves for varying metal ion excess was analysed under the conditions of the so-called corresponding solutions[13-15] according to Eq. (*6*)

$$(pH)_{0c} = m/q(-\log c_M) + \text{const.} \qquad (6)$$

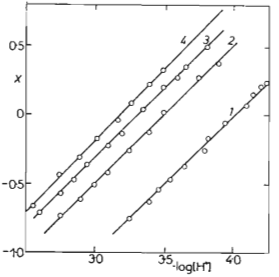

FIG. 7

Logarithmic Analysis of the Absorbance *vs* pH Plots According to Eq. (*5*)

Experimental conditions the same as in Fig. 5; $Y = \log (A - A_L)//\{(A_{01} - (A - A_L)\}$; curves *1* $c_M/c_L = 20$; *2* 80, *3* 150, *4* 200.

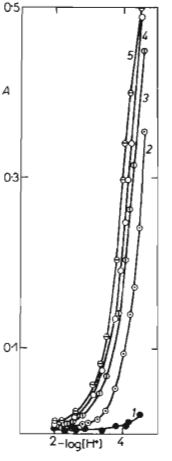

FIG. 8

Absorbance *vs* pH Plots for PCV Solutions with Increasing UO_2^{2+}-Concentration

c_L Fig. 5, 600 nm; curves: c_M/c_L; *1* 1, *2* 20, *3* 80, *4* 150, *5* 200.

The slope was $m/q = 1$ in the broad interval of pH 2·5–4·4. Thus, the equilibrium (B) was proved under the above-mentioned conditions. A similar analysis of absorbance plots at 600 nm for solutions with increasing concentration of uranyl ion gave in turn the value $q = 2$ if $n = 1$. A liberation of two phenolic protons was unambiguously proved, the Eq. (C) had to be checked, since both the equilibria (C) and (D) cannot be distinguished from the absorbance *vs* pH plots for solutions with constant metal ion concentration:

$$2\,M + H_3L \rightleftarrows M_2HL + 2\,H^+ ; \quad {}^*\beta_{12} . \qquad (D)$$

The liberation of the second phenolic proton is, however, responsible for the considerable bathochromic shift of λ_{max} in the UO_2-complex formation. The species with λ_{max} 610–620 nm is formed at pH 3·5–4·5 in solutions with increasing excess of uranyl ion. The bonding of two metal ions was proved according to Eqs (1) and (2) at constant pH 4·2 and 4·0 for solutions with $c_L = 4{\cdot}0 \,.\, 10^{-5}$ and $c_M = (1{\cdot}6–4{\cdot}0) \,.\, 10^{-4}$ or with an even larger excess of metal ion. The plots A *vs* $(ZA - \bar{\varepsilon}_L c_L)/c_M^2$ were straight lines for 560 and 620 nm for $m = 2$ and $n = 1$ only. The simplified loga-

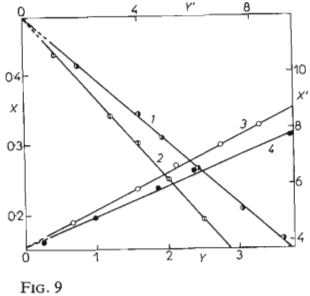

FIG. 9

Analysis of the Increasing Part of the Absorbance *vs* pH Plots *cf.* Fig. 8 According to Eq. (1), (2)

Curves: *1* $c_M/c_L = 200$; $X = A$; $Y = \{(A - A_L)\,[H]^2/c_M^2\} \,.\, 10^4$, *2* $c_M/c_L = 150$; $X = A$; $Y = \{(A - A_L)\,[H]^2/c_M^2\} \,.\, 10^4$, *3* $c_M/c_L = 150$; $X' = (c_L/A) \,.\, 10^5$; $Y' = \{(A - A_L)\,[H]^2/c_M^2 A\} \,.\, 10^5$, *4* $c_M/c_L = 200$; $X' = (c_L/A) \,.\, 10^5$; $Y' = \{(A - A_L)\,[H]^2/c_M^2 \,.\, A\} \,.\, 10^4$.

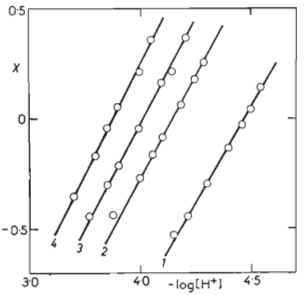

FIG. 10

Logarithmic Analysis of the Absorbance *vs* pH Plots at 600 nm According to Eq. (5)

$X = \log (A - A_L)/\{A_{01} - (A - A_L)\}$; curves: c_M/c_L: *1* 20, *2* 80, *3* 150, *4* 200.

rithmic plot (7):

$$\log \frac{ZA - \bar{\varepsilon}_L C_L}{\varepsilon C_L - n A} = q\,\mathrm{pH} + m \log C_M + \log {}^*\beta_{12} \qquad (7)$$

indicates the successive formation of complexes with M : L = 1 : 1 and 2 : 1 following the increased metal ion concentration. The formation of a dinuclear species was also confirmed by the Asmus plot[22] or indicated on the usual Job curves for the same wavelengths.

Solutions with excess of ligand: The absorbance *vs* pH plots show different shapes for solutions with excess of ligand ($c_L/c_M \sim 1-15$) depending on the acidity and the wavelength (Fig. 12), so that the existence of at least two complexes is evident. The first increasing part of these plots was interpreted by means of transformation (8):

$$c_M/(A - A_L) = \frac{m}{\varepsilon - m\varepsilon_L^*} + \frac{Z^n[H]^q (\varepsilon - n\varepsilon_L^*)^{m-2}}{\left(c_L - n\dfrac{A - A_L}{\varepsilon - n\varepsilon_L^*}\right)(\varepsilon c_M - mA)^{m-1} {}^*\beta'}, \qquad (8)$$

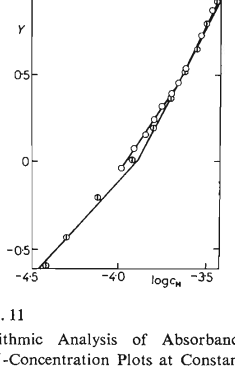

FIG. 11

Logarithmic Analysis of Absorbance *vs* UO_2^{2+}-Concentration Plots at Constant pH According to Eq. (7)

Curves ⊙ pH 4·20; 620 nm, $c_L = 4{\cdot}0 \,.\, 10^{-5}$M; ○ pH 4·00, 560 nm, $c_L = 2{\cdot}0 \,.\, 10^{-5}$M.

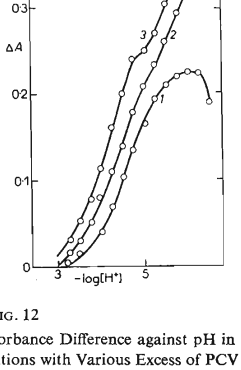

FIG. 12

Absorbance Difference against pH in UO_2^{2+} Solutions with Various Excess of PCV

530 nm, $c_M = 2{\cdot}00 \,.\, 10^{-5}$M. Curves: c_L/c_M: *1* 5, *2* 10, *3* 15.

where $\varepsilon_L^* = \bar{\varepsilon}_L/Z$. Assuming $m = 1$, an equilibrium of the type (E) is to be tested:

$$M + n\,H_3L \rightleftarrows ML_nH_z + q\,H^+ . \qquad (E)$$

Some consumption of the ligand during complexation is respected and the total amount of the ligand is corrected as follows:

$$c_L^* = [c_L - n(A - A_L)/(\varepsilon - n\varepsilon_L)] , \qquad (8a)$$

where A_L is the absorbance of the blank under the same conditions, $Z \to 1$, since the dissociation of the ligand can be neglected in the interpreted pH interval. The simplified transformation (*8*) gives straight lines assuming $q = 1$ (Fig. 13) and this result is fairly confirmed by the logarithmic analysis according to Eq. (*9*) assuming $m = 1$ (Fig. 14)

$$\log\left\{\frac{(A - A_L)\,Z^n}{(\varepsilon - n\varepsilon_L^*)\,c_M - m(A - A_L)}\right\} =$$

$$= q\,\mathrm{pH} + n\log\left(c_L - n\frac{A - A_L}{\varepsilon - n\varepsilon^*}\right) + \log {}^*\beta - (m - 1)\log(\varepsilon - n\varepsilon^*) . \qquad (9)$$

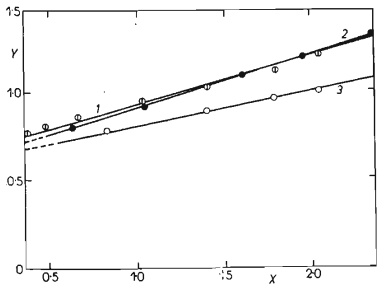

FIG. 13

Analysis of the First Increasing Part of the Absorbance *vs* pH Plots According to Eq. (*8*)

Exp. conditions same as in Fig. 12. Curves: *1* $c_L/c_M = 5$, *2* $c_L/c_M = 10$, *3* $c_L/c_M = 15$; $X = \{(A - A_L)\,[H]/c_L\}.\,10^2$; $Y = c_M.\,10^4/\Delta A$.

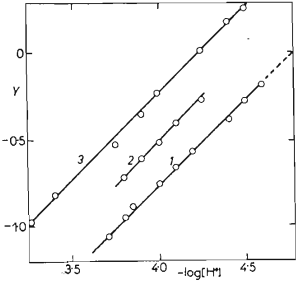

FIG. 14

Logarithmic Analysis of the Absorbance *vs* pH Plots According to Eq. (*9*) (Fig. 12)

$Y = \log \Delta A/(\varepsilon c_M - \Delta A)$.

The corresponding solutions lead to $n/q = 1$ for pH 3·5–4·8 according to the plot (*10*):

$$(\mathrm{pH})_{0c} = n/q(-\log c_L^*) + \text{const.} \qquad (10)$$

Thus, the equilibrium (*B*) is clearly confirmed in solutions with a limited excess of ligand and pH < 4·5.

The second increasing part of the absorbance *vs* pH plot at 600 nm and between pH 5·0–6·5 (Fig. 12) agrees with some of the equilibria of the type (*F*):

$$MH_xL + p\,H_3L \rightleftarrows M(H_xL)_{p+1} + q\,H^+; \quad k_p \qquad (F)$$

for which transformations (*11*) and (*12*) were derived earlier:

$$A - A_L = \varepsilon_2 c_M - \{[Z(A - A_L) - \varepsilon_1 c_M]\,[H]^q/c_L^* k_p\}\,, \qquad (11)$$

$$A - A_L = \varepsilon_1 c_M - \{[Z(A - A_L) - \varepsilon_2 c_M]\,c_L^* k_p/[H]^q\}\,, \qquad (12)$$

where ε_1, ε_2 are molar absorptivities of MH_xL or $M(H_xL)_{p+1}$, respectively. A cor-

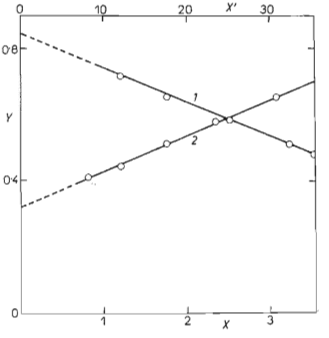

FIG. 15

Analysis of the Second Increasing Part of the, Absorbance *vs* pH Plots According to Eqs (*11*), (*12*)

$c_L = 1{\cdot}00 \,.\, 10^{-4}$M, $c_M = 4{\cdot}00 \,.\, 10^{-5}$M; 600 nm. Curves *1* $X = \{[(A - A_L) - A_{01}] \,.\, [H]/c_L^*\} \,.\, 10^{-3}$; $Y = A - A_L$, *2* $X' = [A_{02} - (A - A_L)]\,[H]^{-1}\,c_L^*$; $Y = A - A_L$.

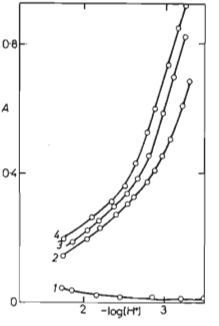

FIG. 16

Absorbance *vs* pH Plots for PCV Solutions in the Presence of Various Excess of Th^{4+}

580 nm, $c_L = 1{\cdot}00 \,.\, 10^{-5}$; *l* 5·0 cm. Curves *1* ligand only, *2* $c_M/c_L = 5$, *3* $c_M/c_L = 10$, *4* $c_M/c_L = 15$.

rected value of c_L was inserted into (*11*) and (*12*):

$$c_L^* = C_L - \frac{[\varepsilon_2 c_M - (A - A_L)] + (p + 1)[(A - A_L) - \varepsilon_1 c_M]}{\varepsilon_2 - \varepsilon_1} \qquad (12a)$$

to respect the ligand consumption during complexation. The transformations (*11*) and (*12*) are straight line plots for $p = 1$ and $q = 1$ only (Fig. 15).

The values of ε_1 and ε_2 from the limiting intercepts were used for a derived logarithmic transformation (*13*):

$$\log \{[Z(A - A_L) - \varepsilon_1 c_M]/[\varepsilon_2 c_M - Z(A - A_L)]\} = \\ = q\ \mathrm{pH} + n \log c_L^* + \log {}^*\beta \qquad (13)$$

The slope of (*13*) $q = 1$ for 600 nm as well as previous results clearly indicate the formation of $UO_2(H_2L)_2$ from UO_2H_2L with the splitting off of one proton from H_3L within the pH values 5·0–6·5. Molar absorptivities for various complexes found from limiting intercepts of particular transformations and the values of the equilibrium constants calculated from logarithmic plots, supposing that the left side of such transformation tends to zero, are summarized in Tables IV and V.

Job Curves for equimolar solutions. The Job curves indicate a single component ratio M : L = = 1 : 1 in the UO_2-complex with PCV at pH 3 and for $c_0 = c_M + c_L = 10^{-3}$, $I = 0{\cdot}1$ and 550 to 600 nm. At pH 4·0 and $c_0 = 5{\cdot}0 \cdot 10^{-4}$ M both complexes with M : L = 1 : 1 and 2 : 1 are indicated at 600 or 550 nm, respectively, which is in good agreement with the results in non-equimolar solutions.

TABLE IV

Molar Absorptivities of Particular Thorium(IV)- or Uranyl(II)-Complexes with Pyrocatechol Violet

The tabulated values are means of at least 4 values for solutions with excess of ligand or metal ion. $I = 0{\cdot}1$ ($NaClO_4$).

Complex	λ, nm	$\varepsilon \cdot 10^{-4}$	Complex	λ, nm	$\varepsilon \cdot 10^{-4}$
Th_2HL	580	1·50[a]	$(UO_2)_2HL$	600	2·40[a]
ThH_2L	580	0·87[a]; 0·86[b]	UO_2H_2L	530	1·57[a]; 1·58[b]
Th_3L_2	580	1·30[b]		600	0·83[b]
Th_4L_3	580	2·05[b]	$UO_2(H_2L)_2$	600	2·12[b]

[a] From the absorbance *vs* pH plot for solutions with metal ion excess; [b] from the absorbance *vs* pH plot for solutions with ligand excess.

TABLE V

Equilibrium (log $*\beta$) and Stability Constants (log β) for Particular UO_2-Complexes with Pyrocatechol Violet

The values are averages of more than 4 values for various excess of ligand or metal ion; $I = 0{\cdot}1$ ($NaClO_4$), $t = 25{\cdot}0 \pm 0{\cdot}2$°C.

Equilibrium	K	log constant
$[MH_2L][H]/[M][H_3L]$	$*\beta_{11}$	$(-0{\cdot}75 \pm 0{\cdot}03)^a$; $(-0{\cdot}72 \pm 0{\cdot}03)^b$
$[M(H_2L)_2][H]/[MH_2L][H_3L]$	$*\beta_{12}$	$-2{\cdot}21^b$
$[M_2HL][H]^2/[H_3L][M]^2$	$*\beta_4$	$-2{\cdot}82 \pm 0{\cdot}10^a$
$[MH_2L]/[M][H_2L]$	β_{11}	$7{\cdot}05^{c,d}$
$[M(H_2L)_2]/[MH_2L][H_2L]$	β_{12}	$5{\cdot}60^{b,e}$
$[M_2HL]/[M]^2[HL]$	β_{21}	$14{\cdot}7^{a,f}$

[a] From the absorbance *vs* pH plots for solutions with metal ion excess; [b] from the absorbance *vs* pH plots for solutions with ligand excess; [c] from the mean of results *a* and *b*; [d] $\beta_{11} = *\beta_{11}/K_{a2}$, [e] $\beta_{12} = *\beta_{12}/K_{a2}$, [f] $\beta_{21} = *\beta_{21}/K_{a2} \cdot K_{a3}$.

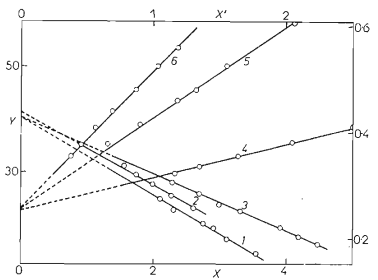

FIG. 17

Analysis of the First Increasing Part of the Absorbance *vs* pH Plots (Fig. 16) According to Eqs (*1*), (*2*)

Curves: *1* $c_M/c_L = 5$; $X = \{(ZA - \bar{\varepsilon}_L c_L) \cdot [H]\} c_M \cdot 10^{-1}$; $Y = A$; *2* $c_M/c_L = 15$; $X' = \{(ZA - \bar{\varepsilon}_L c_L)[H]/c_M\} \cdot 10$; $Y' = A$; *3* $c_M/c_L = 10$; $X' = \{(ZA - \bar{\varepsilon}_L c_L)[H]/c_M\} \cdot 10^{-1}$; $Y' = A$; *4* $c_M/c_L = 15$; $X = \{(ZA - A_L)[H]/Ac_M\}$; $Y = (c_L/A) \cdot 10^6$; *5* $c_M/c_L = 5$; $X' = \{(ZA - A_L)[H]/Ac_M\} \cdot 10^{-2}$; $Y = (c_L/A) \cdot 10^6$; *6* $c_M/c_L = 10$; $X' = [ZA - A_L)[H]/Ac_M$; $Y = (c_L/A) \cdot 10^6$.

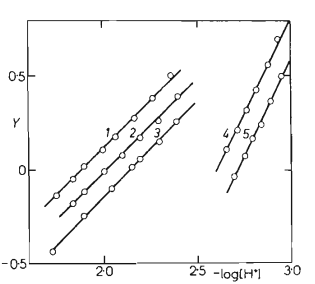

FIG. 18

Logarithmic Analysis of the Absorbance *vs* pH Plots (Fig. 16) According Eq. (*5*)

$Y = \log(ZA - \bar{\varepsilon}_L c_L)/(\varepsilon c_L - A)$. Curves *1*–*3* belong to the first complexation interval *4* and *5* to the second one.

The System Thorium (IV)–Pyrocatechol Violet

The reaction of Th^{4+} with PCV reaches the equilibrium state two hours after mixing the components and soluble coloured compounds are formed at room temperature and in dependence on the acidity and the concentration of components. At pH > 4 a dark precipitate is likely to appear in solution with ligand excess or a pH > 3·5 in those with metal ion excess. There is λ_{max} 530 nm for solutions with ligand excess and at pH < 3·0. New maxima appear with increasing concentration of ligand and larger pH, *i.e.* at 600 and 450—470 nm and in turn two maxima at 450 bm and 530 nm for solutions with low metal ion excess and pH 2·2 on increasing the metal ion concentration the maximum at 530 nm is shifted to 610 nm in acid solutions, whereas the lower-wavelength maximum disappears from pH > 2·5.

Solutions with excess of metal ions. The absorbance *vs* pH plots show at least two complex equilibria with Th^{4+} at 530 nm (Fig. 16). As reported for the system

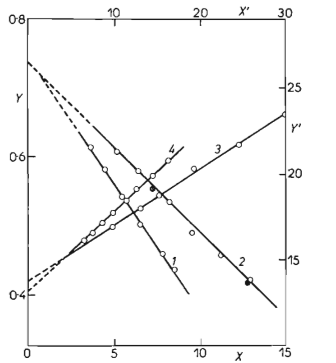

FIG. 19

Analysis of the Second Increasing Part of the Absorbance *vs* pH Plots According to Eqs (*1*), (*2*) (Fig. 16)

Curves: *1* $c_M/c_L = 15$; $X = (ZA - \bar{e}c_L) \cdot [H]^2/c_M^2$; $Y = A$; *2* $c_M/c_L = 10$; $X = (ZA - \bar{e}c_L)\,[H]^2/c_M^2 \cdot 10^{-2}$; $Y = A$; *3* $c_M c_L = 10$; $X' = (ZA - A_L)\,[H]^2/c_M^2 A \cdot 10^{-2}$; $Y' = (c_L/A) \cdot 10^6$; *4* $c_M/C_L = 15$; $X' = (ZA - A_L)\,[H]^2/c_M^2 A \cdot 10^{-1}$; $Y' = (c_L/A) \cdot 10^6$.

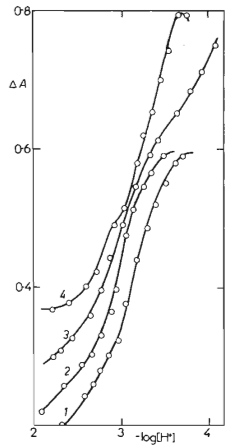

FIG. 20

Absorbance *vs* pH Plots for Th^{4+}-Solutions with Increasing PCV Concentration

580 nm, $c_M = 4{\cdot}00 \cdot 10^{-5}$M (the absorbance of the ligand blanc subtracted). Curves: c_L/c_M: *1* 2·5; 2 5; 3 7·5; *4* 15.

UO_2^{2+} – PCV, the equilibria (B)–(D) were tested with the use of transformations (1)–(3). For the first increasing part of the curves (Fig. 16) at pH 1·7–2·6 the transformations (1), (2) give straight lines for $m = n = q = 1$ (Fig. 17) and $n = 1$ and $q = 1$ were further confirmed by the course and the slope of the logarithmic plot (3) inserting the value of ε_n from the limiting intercepts of (1), (2) (Fig. 18). For the second increasing part of the absorbance *vs* pH plots at pH > 2·6 the transformations (1), (2) gave straight lines for $q = 2$ and $n = 1$ (Fig. 19) and the liberation of two protons was confirmed from the logarithmic plot (3) between pH 2·5–3·5 (Fig. 18).

The interpretation of absorbance *vs* metal ion concentration plot confirms the successive formation of complexes with M : L = 1 : 1 and 1 : 2 at pH ~2·8 and 620 nm. The simplified transformation (2) gave straight line plots A *vs* $(ZA - \bar{\varepsilon}_L c_L)/c_M^2$ for $q = 2$ and $n = 1$ and the logarithmic plot (6) such as $\log(ZA - \bar{\varepsilon}_L c_L)/(\bar{\varepsilon} c_L - nA)$

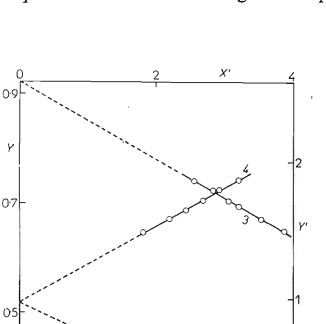

FIG. 21

Analysis of the Successive Increasing Parts of the Absorbance *vs* pH Plots (the Second and Third Complexation Interval) According to Eqs (*11*), (*12*) (Fig. 20)

$c_L/c_M = 15$; Curves: *1* $Y = (A - A_L)$; $X' = [Z(A - A_L) - \varepsilon_1 c_M\,[H]^2/c_L^* \,.\, 10^{-8}$; *2* $Y = (A - A_L)$; $X' = [Z(A - A_L) - \varepsilon_2 c_M]\, C_L/[H]^2$; *3* $Y = (A - A_L)$; $X = [Z(A - A_L) - \varepsilon_1 c_M]\,[H]^2/c_L$; *4* $Y = (A - A_L)$; $X' = [Z(A - A_1) - \varepsilon_2 c_M] \,.\, c_L^*/[H]^2$.

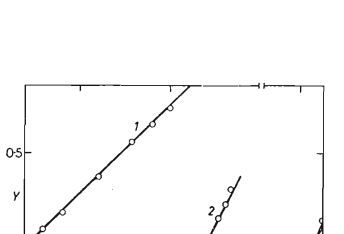

FIG. 22

Logarithmic Analysis of Various Successive Parts of the Absorbance *vs* Acidity Plots According to Eqs (*5*), (*13*) (Fig. 20)

Curves: *1* first complexation interval: $Y = \log[\Delta A/(\varepsilon c_M - \Delta A)]$; *2* second, *3* third complexation interval, $Y = \log[Z(A - A_L) - A_{01}]/[A_{02} - Z(A - A_L)]$.

vs log c_M gives an intersection of two straight lines with slopes $m = 1$ and $m = 2$ from for $10^{-4.4} < c_M < 10^{-4.9}$, respecting the values of molar absorptivity found from extrapolated plot (*2*). Thus the equilibria (*B*) or (*D*) respectively were proved in the particular interval of the metal ion concentration or pH.

Solutions with Excess of Ligand. The absorbance *vs* pH plots for solutions with ligand excess show different shapes in dependence on the ligand excess and wavelength used, *i.e.* 550, 580 and 600 nm. For solutions with $c_L = (1-6) \cdot 10^{-4}$M and $c_L/c_M = 2{\cdot}5-15$ at least two different equilibria are evident depending on pH (Fig. 20). The general equilibria (*E*) and (*G*) were tested by interpretation of various parts of these plots.

$$ML_nH_z + p\,H_3L^- \rightleftarrows ML_{n+p}H_x + q\,H^+ . \qquad (G)$$

The equilibrium (*B*) was confirmed by means of transformations (*6*)–(*11*) at pH 1·6–2·6 (Fig. 21 and 22). With pH > 2·5 the coordination of further ligand species and liberation of two protons per ligand has been confirmed, *i.e.* the equilibrium (*H*):

$$MH_2L + H_3L \rightleftarrows MH_3L_2 + 2\,H^+ . \qquad (H)$$

An analogous equilibrium (*I*) is indicated at pH > 3·3, if the influence of hydrolysis

TABLE VI

Equilibrium (log $*\beta$) and Stability Constant (log β) for Particular Thorium(IV)-Complexes with Pyrocatechol Violet

The values are average of more than four values for various excess of ligand or metal ion; *I* 0·1 ($NaClO_4$), $t = 25{\cdot}0 \pm 0{\cdot}2$°C.

Equilibrium	*K*	log constant
$[MH_2L][H]/[M][H_3L]$	$*\beta_{11}$	$2{\cdot}05 \pm 0{\cdot}03^a$; $2{\cdot}00 \pm 0{\cdot}02^b$
$[MH_3L_2][H]^2/[MH_2L][H_3L]$	$*\beta_{12}$	$-2{\cdot}18 \pm 0{\cdot}04^b$
$[MH_4L_3][H]^2/[MH_3L_2][H_3L]$	$*\beta_{13}$	$-3{\cdot}94 \pm 0{\cdot}02^b$
$[M_2HL][H]^2/[M]^2[H_3L]$	$*\beta_{21}$	$2{\cdot}48 \pm 0{\cdot}03$
$[MH_2L]/[M][H_2L]$	β_{11}	$9{\cdot}83^{c,d}$
$[MH_3L_2]/[MH_2L][HL]$	β_{12}	$15{\cdot}38^{c,e}$
$[MH_4L_3]/[MH_3L_2][HL]$	β_{13}	$13{\cdot}62^{c,f}$
$[M_2HL]/[M]^2[HL]$	β_{21}	$20{\cdot}04^{a,g}$

[a] From the absorbance *vs* pH plots with metal ion excess; [b] from the absorbance *vs* pH plots with ligand excess; [c] the mean of values from *a* and *b*; [d] $\beta_{11} = *\beta_{11}/K_{a2}$, [e] $\beta_{12} = *\beta_{12}/K_{a2}K_{a3}$, [f] $\beta_{13} = \beta_{13}/K_{a2}.K_{a3}$, [g] $\beta_{21} = *\beta_{21}/K_{a2} \cdot K_{a3}$.

is neglected at equilibrium conditions (Fig. 21, 22)

$$MH_3L_2 + H_3L \rightleftarrows MH_4L_3 + 2\,H^+ . \qquad (I)$$

The absorptivities and equilibrium constants for particular complexes are collected in Tables IV and VI.

Job Curves in equimolar solutions. The Job curves for the Th^{4+}-pyrocatechol violet system are indicative only. The species with the component ratio Th : L = 1 : 1 is always evident in solutions at pH 3·0–3·5 and 500–570 nm but the general shape of the curve indicates the formation of a complex with $m > 1$ or $n > 1$ in M_mL_n for $c_0 = 2{\cdot}00 \,.\, 10^{-5}$M, 0·1M sodium perchlorate and 500–570 nm.

DISCUSSION

In the system UO_2^{2+}–PCV the mononuclear complex UO_2H_2L (λ_{max} 550 nm) is formed at pH 2·5–4·3 either in solutions with metal ion excess or a limited ligand excess. In solutions with metal ion excess a binuclear species $(UO_2)_2HL^+$ is also formed especially at pH > 3·5 (λ_{max} 620 nm). Both species are readily hydrolyzed from pH > 4·5, in agreement with previous results on UO_2^{2+} hydrolysis in aqueous solutions[20,21]. In solutions with limited ligand excess the presence of $[UO_2(H_2L)_2]^{2-}$ (λ_{max} 550 nm) becomes evident at pH 5·0–6·5. This complex is then hydrolyzed from pH > 6·5. For the complexes $[UO_2(H_2L)]$ and similarly $[UO_2(LH_2)_2]^{2-}$ there may be some hesitation between the structures (*I*) and (*II*) but there is only one possible bonding scheme in $[(UO_2)_2LH]^{2+}$ (*III*). Some uncertainty remains with respect to the second hydroxylic protons in the catechol nucleus. The libera-

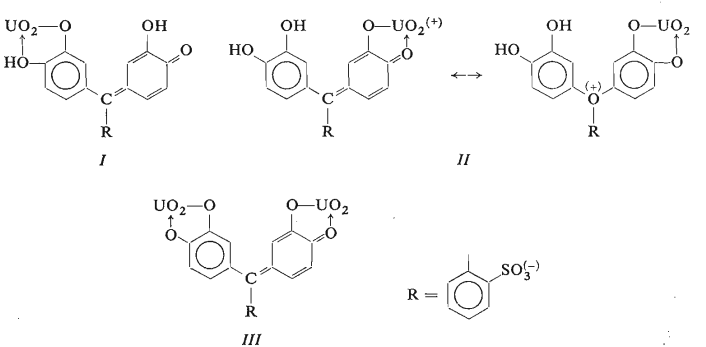

I *II* *III*

tion of the second proton from the *ortho*- or *peri*-dihydroxyl group could not be proved spectrophotometrically during the formation of mononuclear UO_2^{2+} complexes with catechol and derivatives or chromotropic acid. Some problems of UO_2^{2+}-bonding with *ortho*- and *peri*-diphenols were discussed elsewhere[23-25]. Comparing λ_{max} of particular acido-basic ligand forms and the 1 : 1-UO_2 – PCV complex the structure (*II*) is to be preferred to (*I*) in agreement with the similarity between λ_{max} of the complex (530 nm) and the protonated H_4L-form (λ_{max} 550 nm). A similar structure was earlier assumed for the 1 : 1-complex of UO_2^{2+} with Chromazurol S in acidic medium[14]. An 1 : 1-complex of UO_2^{2+} with PCV was also indicated at pH 6·5 in diluted equimolar solutions by Job curves ($c_0 \sim 1 . 10^{-4}$M) but its λ_{max} is 600 nm (see[6]). Thus it seems that a different 1 : 1-chelate is formed under these conditions with the UO_2^{2+} bonding towards the *o*-dihydroxylic group, besides of the dinuclear chelate which predominates in solutions with larger metal ion concentrations.

A similar complexation scheme was observed for the Th^{4+} – PCV system in acid solutions if the own complicated hydrolysis of Th^{4+} is prevented[26]. A mixture of the binuclear complex Th_2HL^{5+} (λ_{max} 610 nm) with ThH_2L^{2+} (λ_{max} 450 and 530 nm) is formed from which the mononuclear species predominates at pH < 2·6 in solution either with metal ion or limited ligand excess. In solution with limited ligand excess the mononuclear species is successively converted into $ThH_3L_2^-$ and $ThH_4L_3^{4-}$ (λ_{max} 600 nm) but two protons are always liberated in this case per one H_3L^- and the number of ligand species in the chelate does not influence the λ_{max} and only slightly the molar absorptivity of metal chelates.

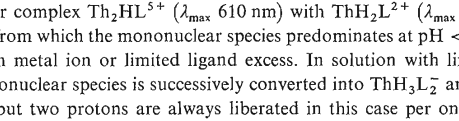

ThH_3L_2

IV

The following structure can be adopted *e.g.* for the Th : L = 1 : 2 species *IV*. Even in this case the binding of the quinoid group is more probable in the 1 : 1-complex but the *o*-diphenolic group of the other nucleus takes rather part in bonding in the higher complex species (2 protons are clearly liberated). The λ_{max} 600 nm is similar to the λ_{max} of the HL^{3-} and L^{4-} forms of the ligand in alkaline medium. There is some ambiguity with the 1 : 3-complex of Th^{4+} with PCV but it seems that this complexation scheme with three mononuclear complexes of Th^{4+} with PCV being successively formed is indirectly confirmed by the previous results of Bartušek for the catechol–Th^{4+} system[27] although the formation of binuclear species of Th^{4+} with catechol and other polyphenols cannot be excluded[27-29].

REFERENCES

1. Vodák Z., Leminger O.: This Journal *19*, 925 (1954).
2. Ryba O., Cífka J., Malát M., Suk O.: This Journal *21*, 349 (1956).
3. Ryba O., Cífka J., Ježková D., Malát M., Suk V.: Chem. listy *51*, 1462 (1957).
4. Suk V., Malát M.: Chemist-Analyst *45*, 30 (1956).
5. Suk V., Malát M.: Chemie *9*, 195 (1957).
6. Mushran S. P., Om Prakash, Awasthi J. N.: Proc. Nat. Acad. Sci. India *37A*, 214 (1967).
7. Prévost M. J.: J. Chim. Phys. *64*, 1533 (1967).
8. Svach M.: Z. Anal. Chem. *149*, 414 (1956).
9. Cífka J., Malát M., Suk V.: Chem. listy *49*, 1792 (1955).
10. Kuivila H. B.: J. Phys. Chem. *59*, 1028 (1955).
11. Paul M. A., Long F. A.: Chem. Revs *57*, 1627 (1960).
12. Sommer L., Kučerová J., Procházková H., Hniličková M.: Publ. Fac. Sci. Univ. Brno *1965*, No. 464, 249.
13. Sommer L., Kubáň V.: This Journal *32*, 4355 (1967).
14. Chiacchierini E., Šepel T., Sommer L.: This Journal *35*, 794 (1970).
15. Sommer L., Kubáň V., Havel J.: Folia Fac. Sci. Univ. Brno, Vol. *11*, Part 1 (1970), (Chemia 7).
16. Malát M.: This Journal *26*, 1877 (1961).
17. Saginašvili R. M., Petrašen V. I.: Ž. Anal. Chim. *22*, 826 (1967).
18. Mustafin I. S., Molot L. A., Archangelskaja A. S.: Ž. Anal. Chim. *22*, 1514 (1967).
19. Wang E. K., Sung Chung Kuo: Chem. Abstr. *64*, 13761 (1966).
20. Dunsmore H. S., Hietanen S., Sillén L. G.: Acta Chem. Scand. *17*, 2644 (1963).
21. Bartušek M., Sommer L.: Z. Anorg. Allgem. Chem. *226*, 309 (1964).
22. Asmus E.: Z. Anal. Chem. *178*, 104 (1960/61).
23. Sommer L., Šepel T., Kuřilová L.: This Journal *30*, 3834 (1965).
24. Sommer L., Šepel T., Kuřilová L.: This Journal *30*, 3426 (1965).
25. Sommer L., Bartušek M.: Folia Fac. Sci. Univ. Brno, Vol. *7*, Part 5 (1966), (Chemia 4).
26. Hietanen S., Sillén L. G.: Acta Chem. Scand. *22*, 265 (1968).
27. Bartušek M.: Publ. Fac. Sci. Univ. Brno *1970*, No 517, 397.
28. Murakami I., Martell A. E.: Bull. Chem. Soc. Japan *29*, 1077 (1966).
29. Martell A. E.: J. Am. Chem. Soc. *82*, 5605, 5608, 5610 (1960).
30. Birjuk E. A., Ravickaja R. V.: Ž. Anal. Chim. *25*, 576 (1970).